Vaporization of Kitaev Spin Liquids

Joji Nasu,[1] Masafumi Udagawa,[2] and Yukitoshi Motome[2]

[1]*Department of Physics, Tokyo Institute of Technology, Ookayama, 2-12-1, Meguro, Tokyo 152-8551, Japan*
[2]*Department of Applied Physics, University of Tokyo, Hongo, 7-3-1, Bunkyo, Tokyo 113-8656, Japan*

The quantum spin liquid is an exotic quantum state of matter in magnets. This state is a spin analog of liquid helium that does not solidify down to the lowest temperature due to strong quantum fluctuations. In conventional fluids, the liquid and gas possess the same symmetry and adiabatically connect to each other by bypassing the critical end point. We find that the situation is qualitatively different in quantum spin liquids realized in a three-dimensional Kitaev model; both gapless and gapped quantum spin liquid phases at low temperatures are always distinguished from the high-temperature paramagnet (spin gas) by a phase transition. The results challenge the common belief that the absence of thermodynamic singularity down to the lowest temperature is a symptom of a quantum spin liquid.

A magnetic state called the quantum spin liquid (QSL), where long-range ordering is suppressed by quantum fluctuations, is a new state of matter in condensed matter physics [1]. Tremendous efforts have been devoted to the realization of the QSL, and several candidates were recently discovered in quasi two-dimensional (2D) and three-dimensional (3D) compounds [2–6]. In these compounds, the QSL is usually identified by the absence of anomalies in the temperature (T) dependence of physical quantities. Namely, it is implicitly supposed that a spin "gas" corresponding to the high-T paramagnet is adiabatically connected with the QSL. This common belief lends itself to the fact that liquid and gas are adiabatically connected with each other in conventional fluids. In fact, the concept of the QSL was originally introduced on the analogy of helium in which the liquid phase is retained down to the lowest T due to strong quantum fluctuations [7].

In general, however, liquid and gas are distinguished by a discontinuous phase transition, while the adiabatic connection between them is guaranteed beyond the critical end point. Hence, a phase transition separating paramagnet and the QSL is also expected. Nevertheless, the theory for thermodynamics of QSLs has not been seriously investigated thus far, and a thermodynamic phase transition for a QSL has not ever been reported beyond the mean-field approximation. It is highly nontrivial whether a liquid-gas transition exists in quantum spin systems in a similar manner to that in conventional fluids. The issue is critical not only for theoretical understanding of QSLs but also for the interpretation of existing and forthcoming experiments.

The lack of theoretical investigation of thermodynamics of QSLs is mainly due to the following two difficulties. One is the scarcity of well-identified QSLs. It is hard to characterize the QSL because spatial quantum entanglement and many-body effects are essential for realizing the QSL [8,9]. The other difficulty lies in less choice of

effective theoretical tools. Any biased approximation might be harmful for taking into account strong quantum and thermal fluctuations.

In this Letter, we solve these difficulties by investigating a 3D extension of the Kitaev model [10], which supports well-identified QSLs as the exact ground states [11], by applying an unbiased quantum Monte Carlo (MC) simulation without a negative sign problem. By clarifying the phase diagram in the whole parameter space, we show that both the gapped and gapless quantum spin liquid phases exhibit a finite-temperature phase transition to the high-temperature paramagnet. The results unveil that the "vaporization" of the quantum spin liquids are quantitatively different from the conventional liquid-gas transition.

The Kitaev model is a quantum spin model with anisotropic exchange interactions for nearest neighbor spins, whose Hamiltonian is given by

$$\mathcal{H} = -J_x \sum_{\langle ij \rangle_x} \sigma_i^x \sigma_j^x - J_y \sum_{\langle ij \rangle_y} \sigma_i^y \sigma_j^y - J_z \sum_{\langle ij \rangle_z} \sigma_i^z \sigma_j^z. \quad (1)$$

Here, σ_i^x, σ_i^y, and σ_i^z are Pauli matrices describing a spin-$1/2$ state at a site i; J_x, J_y, and J_z are exchange constants [10]. This model was originally introduced on a honeycomb lattice shown in Fig. 1(a). The interactions J_x, J_y, and J_z are defined on three different types of the nearest neighbor bonds, x (blue), y (green), and z bonds (red), respectively [see Fig. 1(a)]. This model is exactly solvable by introducing Majorana fermions [10]. The ground state of the Kitaev model is a QSL, where spin-spin correlations vanish except for nearest neighbors [12]. The ground state phase diagram consists of gapless and gapped QSL phases [10], as shown in Fig. 1(c). The QSL with gapless excitation is stabilized in the center triangle including the isotropic case $J_x = J_y = J_z$, while the QSL with an excitation gap appears in the outer three triangles with anisotropic
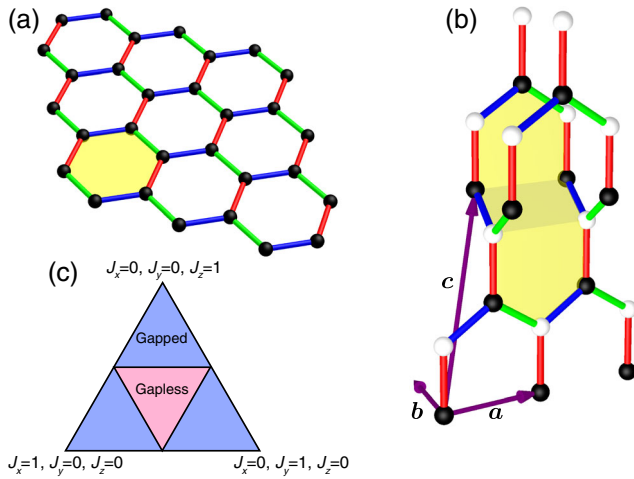
FIG. 1 (color online).   (a) Two-dimensional honeycomb lattice and (b) three-dimensional hyperhoneycomb lattice. Blue, green, and red bonds denote the exchange couplings J_x, J_y, and J_z in the Kitaev Hamiltonian, respectively. The shaded plaquette on each lattice represents the shortest loop p for which the Z_2 variable W_p is defined. a, b, and c represent the primitive translation vectors. (c) Phase diagram of the Kitaev model at zero temperature, common to the models on the honeycomb and on the hyperhoneycomb lattices. This diagram is depicted on the plane where the condition $J_x + J_y + J_z = 1$ is satisfied. There are two kinds of phases, gapped and gapless spin liquids distinguished by the excitation gap.

interactions. The model has been studied not only from the mathematical virtue of the exact solvability but also from the experimental relevance to some Ir oxides [13].

A 3D extension of the Kitaev model is defined on the hyperhoneycomb lattice shown in Fig. 1(b) [11]. This model has relevance to recently discovered iridates Li$_2$IrO$_3$ [14,15]. There are three types of nearest neighbor bonds in this lattice as in the honeycomb lattice. Many fundamental aspects in the 3D Kitaev model are inherited from the original 2D one, including the exact solvability. In particular, the ground state phase diagram is completely the same as that in two dimensions in Fig. 1(c) [11]. On the other hand, the difference in the spatial dimension may matter to finite-T properties; while no phase transition is expected at a finite T for the 2D Kitaev model [16–18], we may anticipate a finite-T phase transition in the 3D case.

We investigate the thermodynamic properties of the 3D Kitaev model by adopting a MC simulation. Since the model given in Eq. (1) is defined on the bipartite lattices, the conventional quantum MC method on the basis of the Suzuki-Trotter decomposition can be applied at first glance. However, due to the bond-dependent interactions in the Kitaev model, the method suffers from the negative sign problem. To avoid the problem, we use an alternative MC method as described below. By applying the Jordan-Wigner transformation [21–23] and rewriting the resulting spinless fermions by Majorana fermions, the Hamiltonian is written in the form

$$\mathcal{H} = iJ_x \sum_{x \text{ bonds}} c_w c_b - iJ_y \sum_{y \text{ bonds}} c_b c_w - iJ_z \sum_{z \text{ bonds}} \eta_r c_b c_w, \quad (2)$$

where c and $\bar{c}$ are the Majorana fermion operators, and $\eta_r = i\bar{c}_b \bar{c}_w$ are Z_2 variables defined on each z bond (r is the bond index): the eigenvalues are ± 1 [22]. As the hyperhoneycomb lattice is bipartite, we term black (b) and white (w) sites so that, on each x bond, the smaller (larger) i site corresponds to the white (black) site, where the numbering for sites is done along chains consisting of x and y bonds, as shown in Fig. 1(b). The Hamiltonian in Eq. (2) is a free Majorana fermion system coupled with the Z_2 degree of freedom $\{\eta_r\}$ on each z bond. Formally, the model is similar to the double-exchange model with Ising localized spins. This allows us to apply the MC algorithms developed for the double-exchange models. Here, we adopt the conventional algorithm in which the MC weight for a given configuration of $\{\eta_r\}$ is obtained by the exact diagonalization of the Majorana fermions [24]. We impose the open boundary conditions for the a and b directions and the periodic boundary condition for the c direction to avoid a subtle boundary problem intrinsic to the Jordan-Wigner transformation [see Fig. 1(b)]. The cluster size $N = 4L^3$, in which the calculations are performed, is taken up to $L = 6$. The details of calculation methods are given in the Supplemental Material [18].

Figure 2(a) shows the T dependence of the specific heat C_v for the isotropic case with $J_x = J_y = J_z = 1/3$. There are two peaks in C_v. The high-T peak at $T \sim 0.6$ does not show the size dependence. On the other hand, the low-T peak located at $T \sim 0.004$ grows with increasing the system size as shown in Fig. 2(b). This is a signature of the phase transition between the low-T QSL phase and the high-T paramagnetic state, as firmly supported by the perturbation arguments below. The size extrapolation of the peak temperature T_c' gives the estimate of the critical temperature in the thermodynamic limit as $T_c = 0.00519(9)$ [see the inset of Fig. 2(b)] [25]. In contrast, the 2D Kitaev model does not show such a growing peak in the specific heat, indicating the absence of the finite-T phase transition [18].

By performing the simulation for various sets of J_x, J_y, and J_z, we obtain the finite-T phase diagram of the 3D Kitaev model. The results are summarized in Fig. 3. Figure 3(a) shows T_c as a function of the anisotropy parameters α and α' shown in the inset [Fig. 3(b) is the log plot of the same data]. The critical temperature T_c takes the maximum value at $\alpha \simeq 1$ corresponding to the isotropic case, and decreases to zero as $\alpha \to 0$ and $\alpha \to 3/2$. The limit of $\alpha \to 0$ corresponds to $J_z \to 1$ with $J_x = J_y = J \to 0$. This limit was discussed by MC simulation for the effective model obtained by the perturbation theory in terms of J/J_z [26]. A finite-T transition was found at $T_c = \tilde{T}_c \times 7J^6/(256J_z^5)$ with $\tilde{T}_c = 1.925(1)$. This asymptotic form of T_c is plotted by the solid lines in Figs. 3(a) and 3(b). It shows fairly good agreement with the
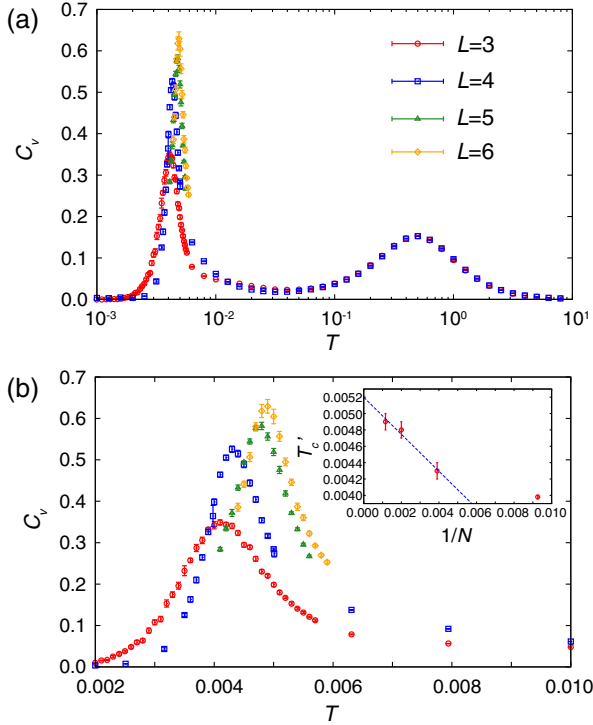
FIG. 2 (color online). (a) Temperature dependence of the specific heat in the isotropic case with $J_x = J_y = J_z = 1/3$ ($\alpha = 1$). (b) The enlarged view in the vicinity of the low-temperature peak. The calculations were performed for the systems on the hyperhoneycomb lattice with $N = 4L^3$ spins up to $L = 6$. The inset in (b) shows the peak temperature T'_c of the specific heat as a function of the inverse of the system size N. The dotted line represents the linear fit for the three largest N.

FIG. 3 (color online). Finite-temperature phase diagram of the 3D Kitaev model. (a) Cut of the phase diagram along the α and α' axes shown in the insets. Log-scale plot for (a) is shown in (b). The solid (dashed) line is the α dependence of T_c obtained by the perturbation expansion in terms of J/J_z (J_z/J), where $J = J_x = J_y$. (c) 3D plot of the phase diagram in the whole parameter space. The base triangle represents the ground state phase diagram shown in Fig. 1(c).

present MC results in the small α region, which strongly supports that T_c estimated from the anomaly in C_v is indeed the critical temperature between the low-T QSL and high-T paramagnet. Meanwhile, in the limit of $\alpha \to 3/2$, by using the perturbation expansion in terms of J_z/J, we find that T_c is scaled by J_z^4/J^3 [18]. The dashed lines in Figs. 3(a) and 3(b) represent the fitting of MC data by this asymptotic scaling. It also well explains the MC data, supporting the phase transition at T_c.

Figure 3(c) summarizes the MC estimates of T_c in the 3D plot. In the entire parameter space, the low-T QSL is separated from the high-T paramagnet by the thermodynamic singularity at T_c. There is no adiabatic connection between the two states, and the transition always appears to be continuous within the present calculations. These are in sharp contrast to the situation in conventional fluids where liquid and gas are adiabatically connected with each other beyond the critical end point in the phase boundary of the discontinuous transition. Thus, the thermodynamics of the QSLs is not understood by the conventional theory for liquids.

Interestingly, the value of T_c becomes maximum at $\alpha \simeq 1$: the QSL phase is most stable against thermal fluctuations
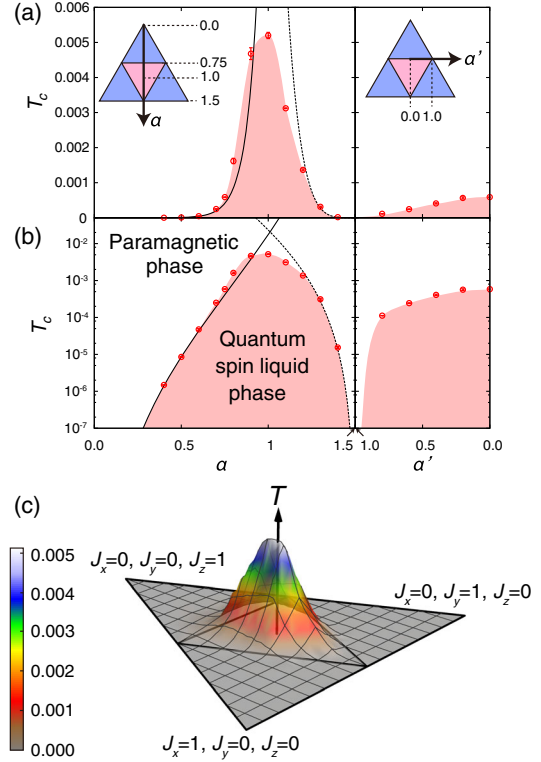
in the isotropic case. The bond-dependent interactions in the Kitaev model compete with each other; it is not possible to optimize the exchange energy on the x, y, and z bonds simultaneously. The frustration becomes strongest at $\alpha = 1$. Hence, interestingly, our MC results in Fig. 3(c) show that the frustration tends to stabilize the QSL against thermal fluctuations. This frustration effect is opposite to that on conventional magnetically ordered states where frustration suppresses the critical temperatures.

In the vicinity of $\alpha = 1$, the ground state is the gapless QSL. By decreasing α, the ground state changes into the gapped QSL at the quantum critical point at $\alpha = 3/4$, as shown in Fig. 1(c). However, T_c changes smoothly around $\alpha = 3/4$, as shown in Fig. 3. Also, we find no singularity in the T dependence of C_v around $\alpha = 3/4$ within the present precision, except for T_c [e.g., see Fig. 4(a)]. In the low-T limit, however, there should be some anomaly in C_v, reflecting the change of low-energy excitations. The results suggest that such anomaly will happen to be seen at much lower T than 10^{-4}.

Now let us discuss the reason why the specific heat C_v exhibits two peaks. We show the T dependence of the
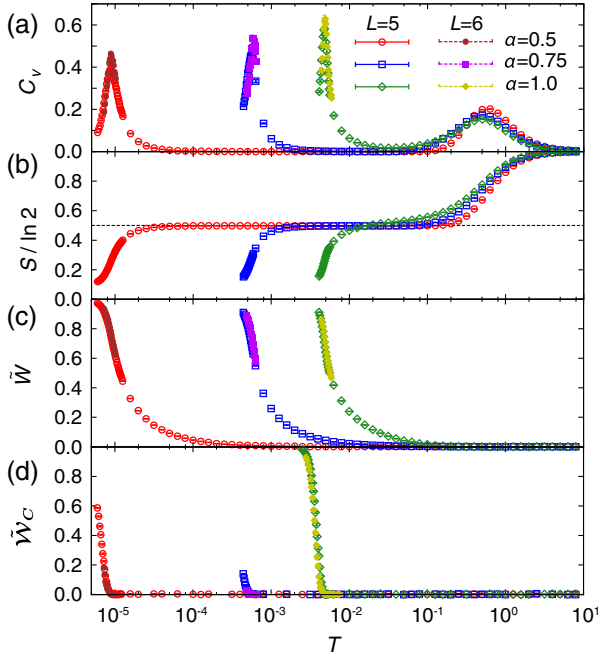
FIG. 4 (color online). Temperature dependences of (a) the specific heat, (b) entropy, (c) Z_2 variables W_p per ten-site plaquette $\tilde{W}$, and (d) the Wilson loop $\tilde{\mathcal{W}}_C$.

entropy per site S in Fig. 4(b), obtained by the numerical integration of C_v divided by T. By decreasing T, the entropy decreases from $\ln 2$ corresponding to the high-T peak in C_v and approaches $\frac{1}{2}\ln 2$. In the T region between the two peaks in C_v, the entropy stays at $\simeq \frac{1}{2}\ln 2$. As further decreasing T, the entropy rapidly deceases again corresponding to the low-T peak in C_v, and approaches zero toward $T = 0$. The successive entropy release is ascribed to a separation of the energy scales for the Majorana fermions and the Z_2 variables η_r. Namely, while decreasing T, the entropy of $\frac{1}{2}\ln 2$ associated with Majorana fermions is first gradually released at $T \sim 0.1$–1, corresponding to their kinetic energy scale $\sim J_x + J_y + J_z = 1$. Subsequently, the remaining entropy of $\frac{1}{2}\ln 2$, associated with the Z_2 variables, is released at the phase transition. This lower energy scale is set by the effective interactions between the Z_2 variables mediated by Majorana fermions, which depend on the anisotropy of the system. We confirm this picture by calculating $\tilde{W}$ defined as the thermal average of the density of the Z_2 variables $W_p = \pm 1$ for each ten-site loop [see Fig. 1(b)], which is computed by the product of η_r [18]. Figure 4(c) shows the T dependence of $\tilde{W}$. This quantity rapidly increases at the lower-T peak in C_v as T decreases. Therefore, the entropy of $\frac{1}{2}\ln 2$ is released according to the coherent growth of W_p at T_c.

However, it is worth noting that the phase transition at T_c is not caused by the symmetry breaking in terms of the local variables W_p. Instead, the phase transition will be understood by the topological nature of excited states as follows.

The excited states are generated by flipping W_p from the ground state where all $W_p = +1$. The flipped $W_p = -1$ form loops because of the local constraints originating from the fundamental spin-1/2 algebra [11]. The excitation energy of loops and their configurational entropy compete with each other, which may lead to the phase transition at a finite T, as is discussed by Peierls for the 2D Ising model [27]. This picture was indeed confirmed in the limit of $J_z \gg J_x, J_y$, through the winding number defined for W_p [26]. In the present case, however, the winding number cannot be defined, as the calculations are done under the open boundary conditions in the a and b directions. Instead, we calculate the thermal average of the Wilson loop along the edge of the ab plane, $\tilde{\mathcal{W}}_C$, which serves as an alternative parameter to the winding number [18]. As shown in Fig. 4(d), $\tilde{\mathcal{W}}_C$ behaves like an order parameter: it becomes nonzero below T_c [25]. The situation is in sharp contrast to the 2D Kitaev model, where the excitation with $W_p = -1$ is allowed independently without local constraints, and, consequently, the QSL is adiabatically connected to the high-T paramagnet.

Our results on the topological transition suggest a new paradigm of critical phenomena beyond the Ginzburg-Landau-Wilson (GLW) theory. Because of the lack of local order parameter, the description based on the GLW theory is no longer applicable to the vaporization of QSLs. Such nontrivial finite-T phase transitions have been studied by the mean-field approximations for 3D Z_2 QSLs on the basis of the Z_2 gauge theory [28,29]. To understand the critical properties, however, it is necessary to take into account fluctuations of a topological structure in the excitations beyond the mean-field approach. The current study presents the first unbiased results on topological transitions, which may give birth to a new concept of critical phenomena beyond the conventional GLW theory.

It will also be interesting to consider the "solidification" of QSLs. Indeed, the solid phase (magnetically ordered phase) is accessible in the context of the present 3D Kitaev model, by considering additional interactions which favor a magnetic order, such as the Heisenberg exchange interaction [30,31]. The detailed study of the magnetic three states of matter, liquid, gas, and solid will provide a new insight in the research area of magnetism.

The present results give a counterexample to the conventional "myth" of QSLs: the absence of phase transition is a requirement for the QSL. This myth has long haunted the experimental identification of QSLs. Our results, however, indicate that a phase transition does not always signal symmetry breaking by a magnetic long-range order. This will urge reconsideration of the experimental detection of QSLs; even if the system exhibits a phase transition, it should not be excluded from the candidates for QSLs, as long as a clear indication of magnetic ordering is not established.

[1] L. Balents, Nature (London) **464**, 199 (2010).
[2] Y. Shimizu, K. Miyagawa, K. Kanoda, M. Maesato, and G. Saito, Phys. Rev. Lett. **91**, 107001 (2003).
[3] S. Nakatsuji *et al.*, Science **309**, 1697 (2005).
[4] J. S. Helton *et al.*, Phys. Rev. Lett. **98**, 107204 (2007).
[5] Y. Okamoto, M. Nohara, H. Aruga-Katori, and H. Takagi, Phys. Rev. Lett. **99**, 137207 (2007).
[6] M. Yamashita, N. Nakata, Y. Senshu, M. Nagata, H. M. Yamamoto, R. Kato, T. Shibauchi, and Y. Matsuda, Science **328**, 1246 (2010).
[7] P. W. Anderson, Mater. Res. Bull. **8**, 153 (1973).
[8] S. Yan, D. A. Huse, and S. R. White, Science **332**, 1173 (2011).
[9] H.-C. Jiang, H. Yao, and L. Balents, Phys. Rev. B **86**, 024424 (2012).
[10] A. Kitaev, Ann. Phys. (Berlin) **321**, 2 (2006).
[11] S. Mandal and N. Surendran, Phys. Rev. B **79**, 024426 (2009).
[12] G. Baskaran, S. Mandal, and R. Shankar, Phys. Rev. Lett. **98**, 247201 (2007).
[13] G. Jackeli and G. Khaliullin, Phys. Rev. Lett. **102**, 017205 (2009).
[14] K. A. Modic *et al.*, Nat. Commun. **5**, 4203 (2014).

[15] T. Takayama, A. Kato, R. Dinnebier, J. Nuss, and H. Takagi, arXiv:1403.3296.
[16] C. Castelnovo and C. Chamon, Phys. Rev. B **76**, 184442 (2007).
[17] Z. Nussinov and G. Ortiz, Phys. Rev. B **77**, 064302 (2008).
[18] See Supplemental Material at http://link.aps.org/supplemental/10.1103/PhysRevLett.113.197205, which includes Refs. [19,20], for details of the calculation method, thermodynamic properties in 2D Kitaev model, and perturbation expansions.
[19] R. H. Swendsen and J.-S. Wang, Phys. Rev. Lett. **57**, 2607 (1986).
[20] K. Hukushima and K. Nemoto, J. Phys. Soc. Jpn. **65**, 1604 (1996).
[21] H.-D. Chen and J. Hu, Phys. Rev. B **76**, 193101 (2007).
[22] X.-Y. Feng, G.-M. Zhang, and T. Xiang, Phys. Rev. Lett. **98**, 087204 (2007).
[23] H.-D. Chen and Z. Nussinov, J. Phys. A **41**, 075001 (2008).
[24] S. Yunoki, J. Hu, A. Malvezzi, A. Moreo, N. Furukawa, and E. Dagotto, Phys. Rev. Lett. **80**, 845 (1998).
[25] The finite-size scalings for C_v and $\tilde{\mathcal{W}}_c$ are not satisfactory for the present data sets, presumably because of the limited system sizes.
[26] J. Nasu, T. Kaji, K. Matsuura, M. Udagawa, and Y. Motome, Phys. Rev. B **89**, 115125 (2014).
[27] R. Peierls, Proc. Cambridge Philos. Soc. **32**, 477 (1936).
[28] T. Senthil and M. P. A. Fisher, Phys. Rev. B **62**, 7850 (2000).
[29] X.-G. Wen, Phys. Rev. B **65**, 165113 (2002).
[30] E. K.-H. Lee, R. Schaffer, S. Bhattacharjee, and Y. B. Kim, Phys. Rev. B **89**, 045117 (2014).
[31] I. Kimchi, J. G. Analytis, and A. Vishwanath, arXiv:1309.1171.